COMPLEMENTARY USE OF OPTICAL METROLOGY AND X-RAY COMPUTED TOMOGRAPHY FOR SURFACE FINISH AND DEFECT DETECTION IN LASER POWDER BED FUSION ADDITIVE MANUFACTURING

Jason C. Fox[1], Felix Kim[1], Zachary Reese[1,2], Christopher Evans[2]
[1]Engineering Laboratory
National Institute of Standards and Technology[*]
Gaithersburg, Maryland, USA
[2]Center for Precision Metrology
University of North Carolina at Charlotte
Charlotte, North Carolina, USA

INTRODUCTION

The development of additive manufacturing (AM) has allowed for production of high-value and complex parts that reduce time-to-market and cost to manufacture [1]. A key benefit of the AM process is the capability to create lattice structures and highly complex, topology optimized parts that reduce weight. Despite this advantage, a limiting factor affecting widespread adoption of AM is the sometimes less desirable as-built surface topography of finished parts compared to those made using traditional manufacturing techniques. As part complexity increases, the ability to alter the surfaces through a secondary operation (i.e., machining or polishing), either in situ or ex situ, decreases [2]. Thus, improvements in the as-built surface texture and understanding its relationship to part quality has been cited as a key need [1,3].

In addition to a stronger understanding of the as-built surface texture of AM parts, development of non-destructive evaluation (NDE) techniques such as x-ray computed tomography (XCT) for surface texture measurement is needed. Traditional surface metrology equipment often requires line of sight or adequate clearance to contact the surface with a stylus, which can be difficult to achieve given the highly complex AM geometries [4]. Townsend et al. presented a methodology to extract areal surface texture from XCT data and compared it with a focus variation (FV) microscopy measurements [5]. Thompson et al. also showed a comparison and alignment of confocal microscopy, coherent scanning interferometry, and FV to XCT data. XCT data in this work was first rotated to align the surface normal to the z-axis via principal component analysis and then translated via commercially available software. The work also suggested the integration of results to improve understanding of complex surface topography measurement [6,7].

The purpose of this research is to investigate the complementary use of optical metrology and XCT for inspection of parts built through laser powder bed fusion (L-PBF) AM, with the primary focus being the benefit that the volumetric XCT data can provide when aligned with the data from conventional surface metrology equipment. Samples made from 17-4 stainless steel (17-4SS) and nickel super alloy 625 (IN625) are measured using a laser confocal (LC) microscope and XCT system. Defects, which include reentrant features on the surface and near surface pores, are identified and located from the XCT data using methodologies described by Fox et al. [8]. The data from the XCT and laser confocal (LC) systems is then aligned using an iterative closest point (ICP) algorithm. This alignment allows for identification of locations in the LC data close to near-surface defects and provides more context for numerical analysis.

METHODOLOGY

Optical Measurements

Surface height data was acquired with a Zeiss LSM 800 LC system. All measurements were performed with a 10x objective and 0.5x tube lens or a 20x objective lens. These settings create

lateral resolutions of 1.25 µm and 0.31 µm, respectively. Measurements were processed with Digital Surf's ConfoMap software to remove outliers and level the surfaces. No other filtering was applied to the data.

XCT Measurements

XCT scans were acquired with North Star Imaging (NSI) CXMM 50 metrological CT system. The system is equipped with a 225 kV source including a tungsten target, a rotary stage, and a 127 μm/pixel flat panel detector (FIGURE 1). The voxel size of the XCT data was 10.9 μm. A typical filtered backprojection algorithm supplied by the vendor was used to reconstruct the dataset [9]. XCT acquisition parameters are shown in TABLE 1, and the methodology for selection of those parameters are detailed in Fox et al [8].

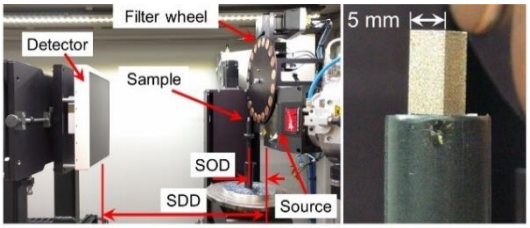

FIGURE 1. (a) XCT system setup, and (b) an example image of the sample.

TABLE 1. XCT acquisition parameters

Parameter	Value
Voltage	160 kV
Current	80 μA
Exposure time	2 s
Filter material/thickness	Cu/4 mm
Number of projection	1000
Source-to-detector distance (SDD)	492.76 mm
Source-to-object distance (SOD)	42.29 mm
Voxel size	10.9 μm x 10.9 μm x 10.9 μm

Experiment Samples

Parts for the analysis were built on the EOS M270 system at the National Institute of Standards and Technology (NIST). Three parts were built for this analysis: two using the commercially available EOS StainlessSteel GP1 (corresponds to US classification 17-4SS [10]) and one EOS NickelAlloy IN625 (corresponds to classification unified numbering system UNS N06625 [11]). It should be noted that the material used for the build was powder reclaimed from prior builds using an 80 µm sieve. It is assumed that the condition of the powder can have a large effect on the surface quality of parts being built and analysis of the powder is currently underway.

For the two parts built using the 17-4SS, the first was built entirely with the default parameters defined by the manufacturer, and will be referred to as "sample 60." The second was built with a laser power of 195 W and laser scan speed of 700 mm/s for the contour passes only (outermost portion of the part) with the rest of the parameters set to the default defined by the manufacturer. This will be referred to as "sample 195". This high power contour setting was chosen because prior work by the authors had shown that these settings create a greater variety of surface features [4,12]. The part built using the IN625 was built with the default parameters defined by the manufacturer and will be referred to as "sample 625." Samples built for the analysis are shown in FIGURE 2.

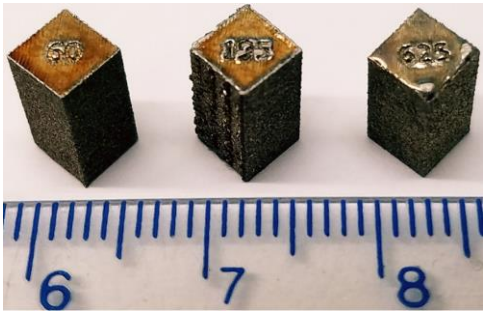

FIGURE 2. Sample 60 (left), sample 195 (center), and sample 625 (right). Scale is in cm.

The samples were built with the same orientation in the build chamber relative to the recoater blade. Surfaces of the samples will be referred to as follows: the top surface is parallel with the build plane and contains the part labels "60," "195," and "625," seen in FIGURE 2. Side surfaces will be referred to using primary intercardinal directions when looking down at the label on the top surfaces. For example, in FIGURE 2, the southeast (SE) and southwest (SW) surfaces of each part can be seen and the northeast (NE) and northwest (NW) surfaces cannot be seen.

RESULTS

Analysis of Optical Metrology Data

Height measurements were taken from the surfaces of the samples using a laser confocal microscope. The sample is aligned in the instrument such that the positive y-axis of the microscope is parallel to the build direction, the intersection of the top surface and left edge of the

sample is at (0,0). Each surface was scanned over a 5 x 5 stitch using a 10x objective and 0.5x tube lens to create a 5.89 mm x 5.89 mm view of the surface with 1.25 µm point spacing. Additionally, each surface was scanned over a 3 x 3 stitch using a 20x objective and 1.0x tube lens to create an 895 µm x 895 µm view of the surface with 0.31 µm point spacing. The scan center was positioned at (2.5,-3) mm.

Analysis of XCT Data

The reconstructed XCT data were imported into VGStudioMAX 3.0 software and the 3-2-1 registration technique available in the software was used to align the orthogonal faces to the same coordinate system and minimize part-to-part variation during the analysis [13]. Then, a stack of images was exported such that the cross-sectional image shows both SW and NE edges of the sample. In addition to the 10.9 µm per voxel resolution, a sub-voxel interpolation to 2.5 µm per voxel was performed through commercially available software and was used to create images for analysis at a higher resolution [14]. From these images, a 2D array of surface heights can be created using the methods described in Fox et al. [8].

Data Alignment

To align the data from various sources, height maps were converted to point clouds and registered using an ICP algorithm, available in the commercially available MATLAB software package. Alignment was performed in multiple steps. For alignment of the 20x LC data and 10x LC data, an initial crop of the 10x LC data is performed to reduce the computational burden of the alignment and limit the search area to the general region where the 20x LC measurement was performed (2.5 mm to the right and 3 mm down from the upper left corner of the surface). From this point, all alignments were completed in two steps. In the first step, the lowest 70 % of points were ignored and the two surfaces are roughly aligned using the ICP algorithm on the highest 30 % of points on the surface. In the second step, the translation and rotation determined in the first step is used as the starting point for the ICP algorithm on the full set of surface points. The alignment was performed using these two steps because even a minor error in selection of a fiducial (on the order of tens of micrometers) can lead to errors in alignment on the order of millimeters in the x and y directions with the ICP algorithm. Aligned sections from the various data sources can be seen in FIGURE 3.

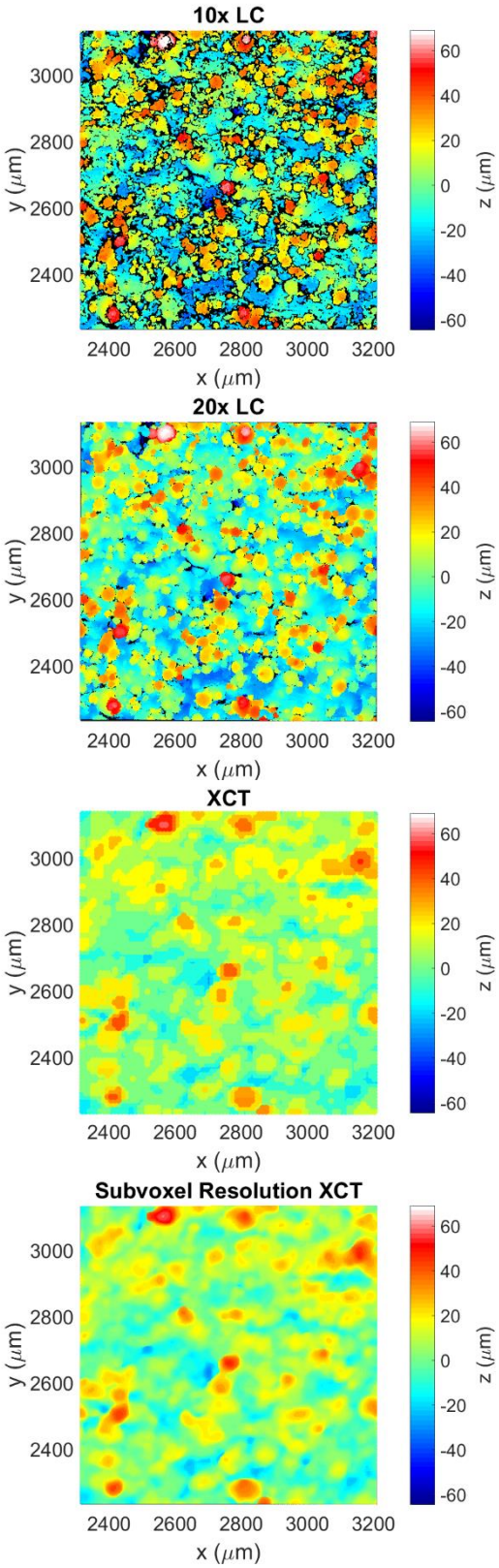

FIGURE 3. Aligned data maps from various sources.

Qualitatively, this method provides good alignment between the various sources. To analyze the quality of the alignment quantitatively, signed distance maps and distributions can be seen in FIGURE 4 through FIGURE 6. Additionally, the signed distances are used to determine the root mean square error (RMSE) between two aligned surfaces. It should be noted that while sub-voxel interpolation of the XCT data to 2.5 µm per voxel is available in the commercial software, it did not exhibit a significant difference in the identification of the surface from the original 10.9 µm per voxel data. This can be seen when comparing FIGURE 5 and FIGURE 6.

Identification of Defects

Images of the surface were taken via scanning electron microscope (SEM) for qualitative comparison. FIGURE 7 shows an example image from the SW surface of sample 60. The image shows a 1 mm x 1 mm area of the surface that encompasses the area previously scanned with the laser confocal microscope using the 20x objective.

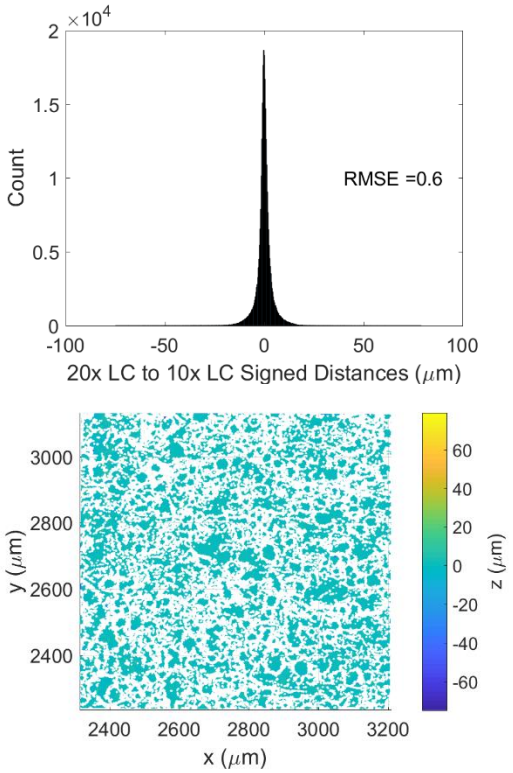

FIGURE 4. Signed distances distribution and map for alignment of the 10x LC and 20x LC data.

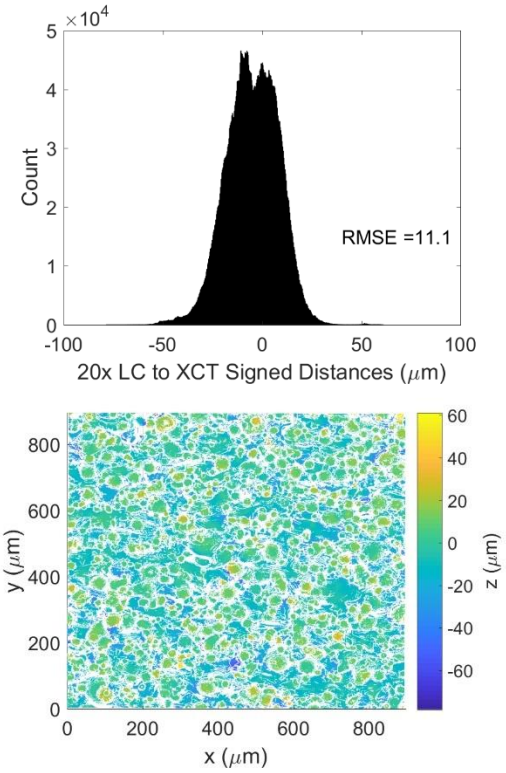

FIGURE 5. Signed distances distribution and map for alignment of the 20x LC and XCT data.

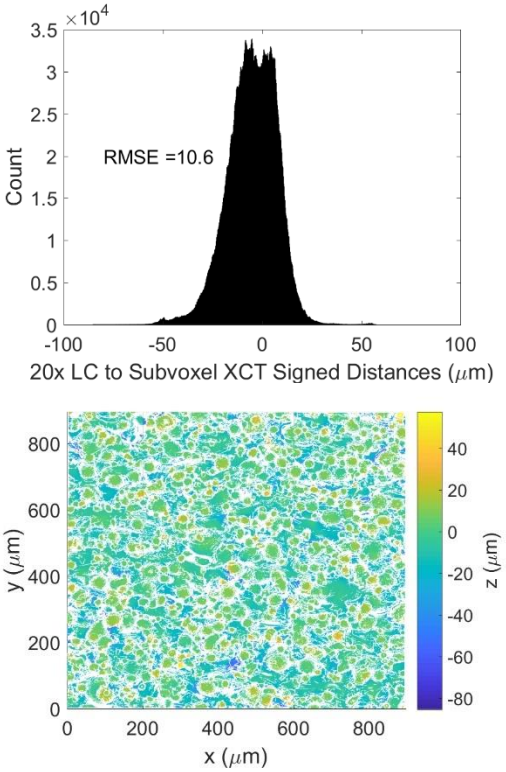

FIGURE 6. Signed distances distribution and map for alignment of the 20x LC and Sub-Voxel XCT data.

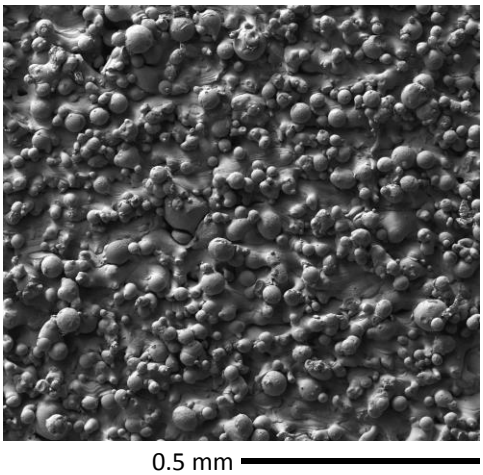

FIGURE 7. SEM image of the SW surface of sample 60.

While the current resolution of the XCT data is limited, it has the distinct advantage of being able to detect pores and undercuts on and near the surface. The method described in Fox et al. [8] was used to determine undercuts on the surface and sub-surface pores from the surface to approximately 275 µm below the surface. The resultant pore and undercut locations are presented in FIGURE 8.

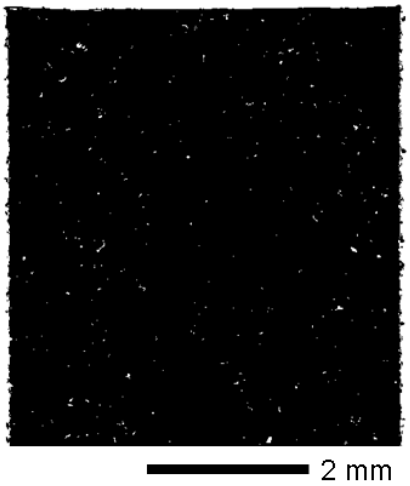

FIGURE 8. Location of near surface pores and undercuts on the SW surface of sample 60 identified from XCT data.

From the identification of pores and undercuts in FIGURE 8, surface data near these defects can be extracted from the previously aligned data sources. Defect locations are overlaid onto the 20x LC data in FIGURE 9. A closer view of the surface data near the rightmost defect location in FIGURE 9 (highlighted with a red box) is shown in FIGURE 10. While this methodology allows us to align and identify regions where subsurface defects exist, it is still inconclusive whether trends in the surface data from the LC system can identify these defects. As such, further analysis of the surface data is ongoing.

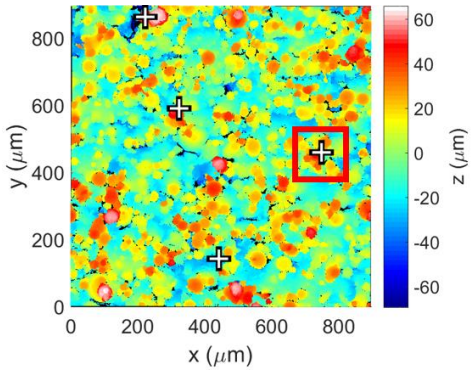

FIGURE 9. Surface data for the SW surface of sample 60, taken via 20x objective on the laser confocal system, with defect areas (pore and undercut locations) indicated by plus signs.

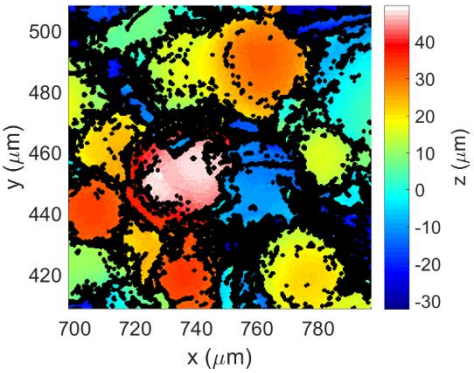

FIGURE 10. Surface data taken via 20x objective on the laser confocal microscope for the rightmost defect area (highlighted with a red box) in FIGURE 9.

CONCLUSIONS

In this work, IN625 and 17-4SS samples were built on a commercially available L-PBF system and analyzed via laser confocal microscope and XCT. The data were aligned using an ICP algorithm for complementary analysis. Pores and undercuts were identified using XCT data, which allowed for more stringent analysis of the surface near these features. However, at 10.9 µm per voxel the current resolution of XCT prevents strong quantitative analysis of the surface data from XCT or relevant comparison to the laser confocal microscope surface data. While quantitative analysis has been performed on XCT data with larger voxel sizes, it has utilized sub-voxel

interpolation. The current analysis has shown that sub-voxel interpolation provided little change in the determined surface, and greater benefit may be derived from proprietary surface determination algorithms in the commercially available software. This was not included in the current analysis.

Future work will include the classification of defects found in the data (i.e., subsurface pores vs undercuts on the surface), and identification of the depth of pores. Additionally, advanced pore detection techniques and image analysis, such as those presented in Kim et al. [15], and sectioning of the samples for comparison to the XCT and laser confocal microscope data are in progress. It is anticipated that this type of analysis will create avenues to get richer information from the surface data and add a potential methodology for feature based metrology.

ACKNOWLEDGEMENTS
This work was performed in part in the NIST Center for Nanoscale Science and Technology (CNST) NanoFab Facility. The authors would like to thank Maxwell Praniewicz for his suggestions to improve the alignment methodology, and North Star Imaging for providing the XCT system through a Cooperative Research and Development Agreement with NIST and allowing the use of the data acquired.

REFERENCES

[1] Measurement Science Roadmap for Metal-Based Additive Manufacturing. Gaithersburg, MD: NIST, US Department of Commerce; 2012.
[2] Pyka G, Burakowski A, Kerckhofs G, Moesen M, Van Bael S, Schrooten J, et al. Surface modification of Ti6Al4V open porous structures produced by additive manufacturing. Advanced Engineering Materials 2012;14:363–70. doi:10.1002/adem.201100344.
[3] America Makes & ANSI Additive Manufacturing Standardization Collaborative Standardization Roadmap for Additive Manufacturing, Public Draft v1.0. 2017.
[4] Fox JC, Moylan S, Lane BM. Preliminary Study Toward Surface Texture as a Process Signature in Laser Powder Bed Fusion Additive Manufacturing. Proceedings of the 2016 ASPE Summer Topical Meeting: Dimensional Accuracy and Surface Finish in Additive Manufacturing, Raleigh, NC: 2016.
[5] Townsend A, Pagani L, Scott P, Blunt L. Areal surface texture data extraction from X-ray computed tomography reconstructions of metal additively manufactured parts. Precision Engineering 2017;48:254–64. doi:10.1016/j.precisioneng.2016.12.008.
[6] Thompson A, Körner L, Senin N, Lawes S, Maskery I, Leach R. Measurement of internal surfaces of additively manufactured parts by X-ray computed tomography. 7th Conference on Industrial Computed Tomography, Leuven, Belgium: 2017.
[7] Thompson A, Senin N, Giusca C, Leach R. Topography of selectively laser melted surfaces: A comparison of different measurement methods. CIRP Annals - Manufacturing Technology 2017. doi:10.1016/j.cirp.2017.04.075.
[8] Fox JC, Kim FH, Reese ZC, Evans C. Investigation of complementary use of optical metrology and x-ray computed tomography for surface finish in laser powder bed fusion additive manufacturing, Leuven, Belgium: 2017, p. 132–6.
[9] L.A. Feldkamp, L.C. Davis, J.W. Kress, Practical cone-beam algorithm, J. Opt. Soc. Am. A 1(6) 612-619. 1984.
[10] Material data sheet - EOS StainlessSteel GP1 for EOSINT M270 2009. https://scrivito-public-cdn.s3-eu-west-1.amazonaws.com/eos/public/5f84f5d2c88ac900/05fb1582834a38c85ef6dd859733a230/EOS_StainlessSteel-GP1_en.pdf (accessed December 7, 2015).
[11] Material Data Sheet - EOS NickelAlloy IN625 2011. http://ip-saas-eos-cms.s3.amazonaws.com/public/d1327facdca0e32a/373a60ec4f5c891b7dbcdf572e37d3b0/EOS_NickelAlloy_IN625_en.pdf (accessed June 13, 2017).
[12] Fox JC, Moylan SP, Lane BM. Effect of Process Parameters on the Surface Roughness of Overhanging Structures in Laser Powder Bed Fusion Additive Manufacturing. Procedia CIRP 2016;45:131–4. doi:10.1016/j.procir.2016.02.347.
[13] Volume Graphics GmbH, VGStudioMax 3.0.
[14] Avizo 9.4, Thermo Fisher Scientific, Waltham, MA.
[15] Kim FH, Moylan SP, Garboczi EJ, Slotwinski JA. Investigation of pore structure in cobalt chrome additively manufactured parts using X-ray computed tomography and three-dimensional image analysis. Additive Manufacturing 2017;17:23–38. doi:10.1016/j.addma.2017.06.011.